Publications

6-2015

Magnetic Flux Circulation in the Rotationally Driven Giant Magnetospheres

P. A. Delamere
University of Alaska, Fairbanks

A. Otto
University of Alaska, Fairbanks

X. Ma
University of Alaska, Fairbanks, max@erau.edu

F. Bagenal
University of Colorado Boulder

R. J. Wilson
University of Colorado Boulder

Follow this and additional works at: https://commons.erau.edu/publication

Part of the Astrophysics and Astronomy Commons

RESEARCH ARTICLE

Correspondence to:
P. A. Delamere,
Peter.Delamere@gi.alaska.edu

Magnetic flux circulation in the rotationally driven giant magnetospheres

P. A. Delamere[1], A. Otto[1], X. Ma [1], F. Bagenal[2], and R. J. Wilson[2]

[1]Geophysical Institute, University of Alaska Fairbanks, Fairbanks, Alaska, USA, [2]Laboratory for Atmospheric and Space Physics, University of Colorado, Boulder, Colorado, USA

Abstract The giant-planet magnetodiscs are shaped by the radial transport of plasma originating in the inner magnetosphere. Magnetic flux transport is a key aspect of the stretched magnetic field configuration of the magnetodisc. While net mass transport is outward (ultimately lost to the solar wind), magnetic flux conservation requires a balanced two-way transport process. Magnetic reconnection is a critical aspect of the balanced flux transport. We present a comprehensive analysis of current sheet crossings in Saturn's magnetosphere using Cassini magnetometer data from 2004 to 2012 in an attempt to quantify the circulation of magnetic flux, emphasizing local time dependence. A key property of flux transport is the azimuthal bend forward or bend back of the magnetic field. The bend back configuration is an expected property of the magnetodisc with net mass outflow, but the bend forward configuration can be achieved with the rapid inward motion of mostly empty flux tubes following reconnection. We find a strong local time dependence for the bend forward cases, localized mostly in the postnoon sector, indicating that much of the flux-conserving reconnection occurs in the subsolar and dusk sector. We suggest that the reconnection occur in a complex and patchy network of reconnection sites, supporting the idea that plasma can be lost on small scales through a "drizzle"-like process. Auroral implications for the observed flux circulation will also be presented.

1. Introduction

The dynamics of the giant-planet magnetospheres are strongly influenced by planetary rotation. The moons of Jupiter and Saturn, Io and Enceladus, respectively, feed plasma into rotating magnetodiscs composed of equatorially confined plasma, carrying currents that distort the magnetic field into a disc-like structure (see reviews by *Kivelson* [2014] and *Delamere et al.* [2014]). The magnetodisc can be described with a two-dimensional equilibrium model [e.g., *Caudal*, 1986; *Achilleos et al.*, 2010; *Chou and Cheng*, 2010] where a current sheet forms in the middle magnetosphere and a more dipolar field forms in the outer magnetosphere (hereafter defined as the magnetic cushion). For sufficiently long temporal averages, the mass produced by the moons must be transported outward through the magnetodisc and lost to the solar wind. This requires a radial transport mechanism for plasma mass and magnetic flux that conserves planetary magnetic flux. But a detailed understanding of the transport physics has proved elusive. The purpose of this paper is to examine the Cassini magnetometer data from 2004 to 2012 and auroral images to describe the nature of outward mass transport and magnetic flux circulation in the giant magnetospheres.

Radial transport can be driven by four forces: (1) gravity, (2) centrifugal stresses, (3) internal plasma energy density, and (4) magnetic tension (e.g., see discussion by *Southwood and Kivelson* [1987] and *Mauk et al.* [2009]). Gravity can be ignored at the orbits of Enceladus and Io as the gravitational potential is small compared with the centrifugal potential. However, the centrifugal potential and the potential associated with internal energy and magnetic tension compete. Centrifugal forces drive outward motion, while the internal energy density (i.e., flux tube entropy) counteracts this motion.

In a low plasma β environment (i.e., ratio of plasma pressure to magnetic pressure), the centrifugal interchange instability has been suggested as a mechanism that facilitates the radial interchange of flux tubes without changing the background magnetic field [*Gold*, 1959]. This instability is akin to the gravitationally driven Rayleigh-Taylor instability where a cold, dense plasma sits radially inward of a hot tenuous plasma and with the outward centrifugal stress replacing gravity. If the mass content per unit magnetic flux, $\eta = \int (\rho/B)\, ds$ (with $V = \int ds/B$ defined as the flux tube volume per unit of magnetic flux), decreases with radial distance

(i.e., $\partial\eta/\partial L < 0$, where L is the radial coordinate), then the plasma torus is centrifugally unstable. Also, the condition $\partial(pV^\gamma)/\partial L < 0$ is unstable with respect to ballooning modes, but the influence of fast rotation on this ballooning condition is unresolved [*Schindler and Birn*, 2004]. However, the flux tube entropy, $S = \int (p^{1/\gamma}/B)ds$, increases with radial distance due to an ever increasing flux tube volume and because the suprathermal tail to the ion distribution dominates the plasma pressure in the middle and outer magnetosphere [*Mauk et al.*, 2004; *Sergis et al.*, 2007, 2009]. In general, $\partial(pV^\gamma)/\partial L > 0$ and the magnetodisc should be stable to centrifugal interchange motion. *Siscoe and Summers* [1981] first discussed the possibility of plasma torus impoundment by "ring currents," indicating that other such factors may be important in radial transport.

In a high plasma β environment, the interchange motion will distort the magnetic field and *Southwood and Kivelson* [2001] and *Kivelson and Southwood* [2005] have argued that ballooning will replace interchange. At both Jupiter and Saturn (coincidentally) the plasma β reaches unity at $L \sim 12$ [*Mauk et al.*, 2004; *Sergis et al.*, 2007]. At Jupiter, $\beta \gg 1$ in the plasma sheet of the middle and outer magnetosphere. The ballooning mode requires a pressure anisotropy with $T_\parallel > T_\perp$ such that the parallel pressure exceeds the combined perpendicular plasma pressure and magnetic field pressure. *Kivelson and Southwood* [2005] argued that at Jupiter, flux tubes rotating from noon to dusk are free to expand outward due to loss of confinement by the magnetopause boundary. The bounce period of 10 s of keV ions (typical for Jupiter's energetic ion population) is comparable to the few hours of flux tube motion from noon to dusk; therefore, the parallel motion is nonadiabatic and the particles tap the centrifugal potential to boost parallel energy where $p_\parallel \approx \rho u_\parallel^2$. *Vogt et al.* [2014] demonstrated the development of this anisotropy (i.e., $T_\parallel > T_\perp$) for an expanding flux tube using a test particle simulation but did not self-consistently evolve the ion distribution to account for possible isotropy through pitch angle scattering.

When considering radial stress balance for Jupiter's magnetodisc, *Paranicas et al.* [1991] examined Voyager particle and magnetic field data in the midnight sector and found that pressure anisotropy was indeed important in the stress balance. A similar study was conducted for Saturn by *Kellett et al.* [2011] showing that pressure gradients are important in the middle and outer magnetosphere and that anisotropy is important in the inner magnetosphere with $p_\parallel < p_\perp$ due to ring beam-type distributions from pickup ions. In this case, ballooning may not be important at the smaller, less energetic magnetosphere of Saturn.

Ultimately, magnetic reconnection must be involved in the transport and flux circulation process. *Vasyliunas* [1983] first described the mass loss process to the magnetotail, involving a magnetic X-line and O-line in the magnetotail region. The reconnection process is facilitated by centrifugal stretching of the magnetodisc into the midnight sector until the current sheet collapses and reconnection operates, releasing a plasmoid down the tail. Plasma on the planetward side of the X-line rotates back to the dayside and escapes down the dusk flank, completing the Vasyliunas cycle.

There is evidence that supports large-scale plasmoid release in the tail as expected in the Vasyliunas cycle. The location of the X-line in the tail region has been verified [*Woch et al.*, 2002; *Vogt et al.*, 2010; *Kasahara et al.*, 2013; *Jackman et al.*, 2014] (but angled sunward instead of tailward) and with evidence of plasmoid formation [*Russell et al.*, 1999; *Kronberg et al.*, 2005; *Hill et al.*, 2008]. However, the frequency of plasmoid formation is inconsistent with the required mass loss from the magnetosphere. *Bagenal* [2007] argued that much of the plasma loss to the tail occurs via small-scale "drizzle" versus large-scale plasmoid formation. *Thomsen et al.* [2014] also confirmed that much of the mass loss at Saturn likely occurs on the dusk flank through drizzle. The question is, If large-scale plasmoids do not form with sufficient frequency in the tail, then where is reconnection operating and why does it elude detection? We will focus on flux circulation at Saturn, identifying regions in the magnetosphere at all local times where reconnection can operate. In this paper we examine experimental evidence at Saturn and consider the consequences at both Saturn and Jupiter.

2. Magnetic Reconnection and Transport

As a basis for our discussion of transport, we will adopt the definition of flux tube entropy, $S = \int (p^{1/\gamma}/B)ds$, to quantify the ordering of magnetospheric flows. The local entropy, $s = p/\rho^\gamma$ (where ρ is the mass density, p is the pressure, and γ is the polytropic index), and flux tube entropy are conserved in ideal MHD; therefore, changes in entropy are associated with nonadiabatic processes, mass loss/gain from flux tubes, heat loss/gain from flux tubes, and/or integrity of a magnetic flux tube [*Wing and Johnson*, 2010]. Magnetospheres are stable to interchange motion provided that the flux tube entropy increases monotonically with radial distance, just as an atmospheric temperature inversion renders the air convectively stable. In the case

of the giant magnetospheres, the internal source of plasma will increase flux tube entropy in the inner magnetosphere and must, at some point, enable outward mass transport.

In addition to sources of plasma, one of the most effective mechanisms for changing flux tube entropy is magnetic reconnection. Thin current sheets, e.g., on the order of the ion inertial length, are necessary for reconnection to operate. Therefore, a key ingredient in magnetic reconnection is understanding the process of current sheet thinning. Considerable attention has been given to current sheet thinning in the near-Earth current sheet during the substorm growth phase [*Otto et al.*, 2014; *Hsieh and Otto*, 2014]. A key component of thinning is the net magnetic flux transport that must occur out of a region with outwardly divergent flows, though other ideal macroinstabilities (e.g., ballooning modes for Rayleigh-Taylor instabilities) are considered too. Following reconnection, the newly formed flux tube planetward of the X-line is depleted of plasma with much of the original plasma content transferred to a plasmoid. The empty flux tube is surrounded by higher-entropy flux tubes and moves inward to a region of equal entropy. This transport process is thought to be the cause of bursty bulk flows found in terrestrial substorm processes [e.g., *Wolf et al.*, 2012; *Birn et al.*, 2011; *Sergeev et al.*, 2012]. Note that reconnection associated with flux circulation at substorm onset starts deep in the closed terrestrial magnetosphere.

Magnetic reconnection can occur when a thin current sheet is established. While much attention has been given to tail reconnection where thin current sheets are expected [e.g., *Jackman et al.*, 2014], magnetic nulls have been found in the dayside magnetodisc, suggesting that magnetic reconnection is operating on *closed* field lines within the centrifugally stretched disc [*Russell et al.*, 1999; *Kivelson and Southwood*, 2005]. *Southwood and Kivelson* [2001] first suggested that the magnetodisc might be subject to ballooning during magnetospheric expansion. We argue this is one mechanism for generating thin current sheets on the dayside; therefore, magnetic reconnection should be expected to occur at any local time and not just in the midnight sector.

Vogt et al. [2011] examined the local time distribution of the normal magnetic field component (B_θ) to the magnetodisc at Jupiter using Galileo magnetometer data. A clear pattern emerges at Jupiter. In the postmidnight sector the normal component is uniformly small, suggesting a frequent presence of thin current sheets. In the postnoon sector, the normal component is significantly larger, suggesting a more dipole magnetic field topology. Yet in the prenoon and premidnight sectors the scatter in the data is significant, showing combination of thin current sheets with more dipolar configurations. These transition regions may also be susceptible to reconnection, motivating our survey of all local times to understand global flux circulation. In the following analysis, we examine Cassini magnetometer (MAG) data to identify thin current sheets and proximity to potential reconnection sites at Saturn.

3. Azimuthal Magnetic Field Bend: Signatures of Reconnection

An azimuthal bend back magnetic field configuration is an expected property of the rotating magnetodisc with mass outflow [*Vasyliunas*, 1983]. Corotation-enforcing radial currents are added to the magnetodisc with radial distance [e.g., *Hill*, 1979; *Ray et al.*, 2010]. However, we note that no significant radial currents are added to Jupiter's magnetodisc beyond 30 R_J [*Khurana*, 2001], suggesting a decoupling of the magnetodisc from the ionosphere in the outer magnetosphere. As plasma flows radially outward, the loss of coupling will drag the magnetic field into a more bent back configuration as the magnetic field evolves Alfvénically. We estimate the effective mass loading that is required to sustain Alfvénic bend back at Saturn in the limit of ionospheric decoupling and negligible solar wind influence (e.g., viscous stresses near the magnetopause boundary).

The plasma outflow speed in Saturn's outer magnetosphere is a nonnegligible fraction of the corotation speed, and plasma beyond ~15R_S is lost from the magnetodisc in less than one rotation [*Bagenal and Delamere*, 2011]. The expected Alfvénic evolution of the magnetic field results in a $\mathbf{J} \times \mathbf{B}$ force balanced by an effective momentum loading source, or

$$\dot{M}\Delta v_\phi = \frac{1}{\mu_o} \int \mathbf{J} \times \mathbf{B} \, dV = \frac{1}{\mu_o} \int B_\phi B_\theta \, dA \tag{1}$$

In the corotating frame, deviations from corotation result in B_ϕ perturbations and Δv_ϕ is the deviation from rigid corotation. The upper limit for the effective mass loading rate, $\dot{M}$, is the plasma mass outflow rate. Using average values of the magnetic field from Cassini magnetometer data in the outer magnetosphere between
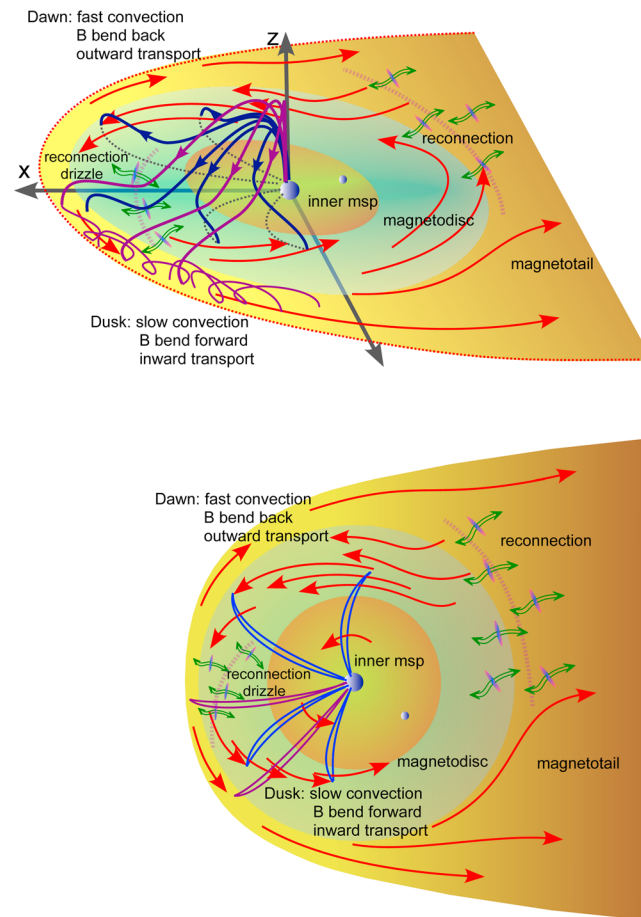
Figure 1. Illustration of the magnetic field topology and flux circulation at Saturn. Flows are shown with red arrows. Magnetic fields are shown in purple (mapping to outer magnetosphere) and blue (showing bend back and bend forward configurations).

15 and 25 R_S (i.e., $B_\phi = 0.5$ nT and $B_{\theta,\text{dipole}} \sim 2$ nT), average deviation from corotation $\sim$100 km/s, and integrating over the cylindrical cross section of the magnetodisc, the mass transport rate is roughly 70 kg/s. This is consistent with mass outflow rates from physical chemistry models (e.g., $\sim$60 kg/s [*Fleshman et al.*, 2013]), suggesting that the bend back in the outer magnetosphere may not be due to ionospheric coupling currents.

If reconnection occurs within the magnetodisc, then the reconnection flows from the X-line will further modify the azimuthal bend of the magnetic field due to variations in the azimuthal component of the velocity. On the planetward side of the X-line, rapid inflows combined with conservation of angular momentum could, in principle, cause a bend forward configuration if the inflow channel can penetrate sufficiently deep into the inner magnetosphere (see Figure 1). The penetration distance is dependent on the entropy of the newly formed flux tube discussed above. Similarly, radial outward flow from the X-line can enhance the magnetic field bend back. The problem of azimuthal bend is further complicated by the fact that reconnecting field lines have different angular velocities. For instance, field lines in the outer magnetosphere rotate slower than field lines in the inner magnetosphere due to a breakdown in corotation. If reconnection operates across these field lines, then the angular velocity of newly reconnected field lines close to the reconnection site decreases while flux is accelerated planetward and angular momentum conservation tends to reaccelerate flux tubes. Figure 2 illustrates the angular momentum transport during reconnection where ω_5 in the inner magnetosphere is greater than ω_1 in the outer magnetosphere (black profile). Following reconnection, the local meridian has a radial angular velocity profile shown in red and the mixing of angular momentum will affect the azimuthal magnetic field component. As a guiding principle in our analysis below, we will use the ratio $|B_\phi|/|B| > 0.5$ to evaluate the likely proximity of the Cassini spacecraft to reconnection sites because of a possible thin current sheet and because of enhanced bend forward/back due to magnetic reconnection.
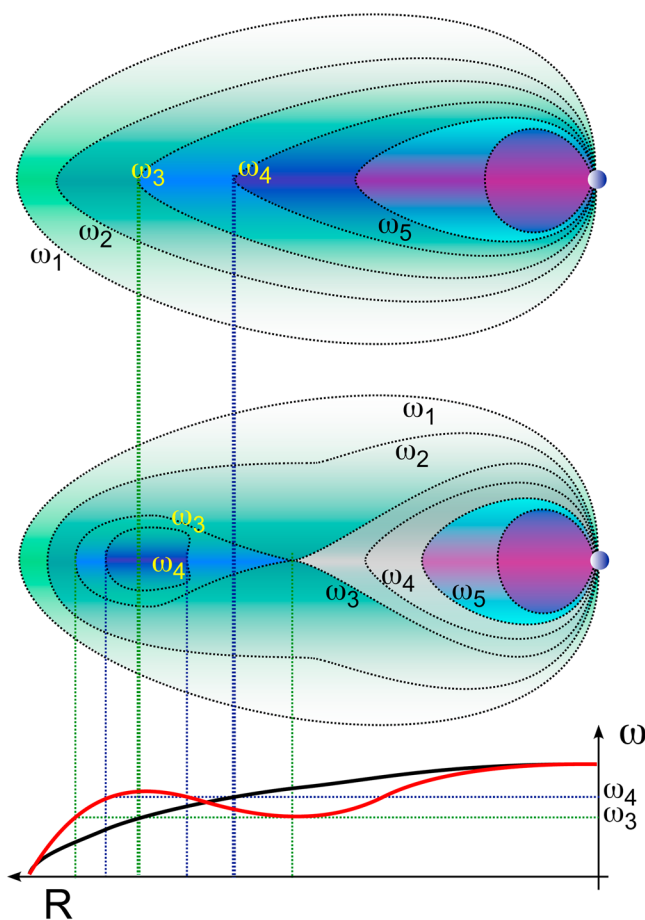
Figure 2. An illustration of angular momentum transport during reconnection on closed field lines. The illustration shows the effect of mixing angular velocities (ω) during reconnection for the initial radial profile shown in black. The resulting angular velocity profile is shown in red. Subsequent evolution of this profile would be subject to angular momentum conservation during radial flow.

We note that any local perturbation to flow, e.g., reconnection, will significantly perturb the local magnetic field following the Walén relation, $\delta B/B_o = v_{flow}/v_{Alfvén}$. Because reconnection outflows are expected to be $\sim v_{Alfvén}$, significant perturbations are expected.
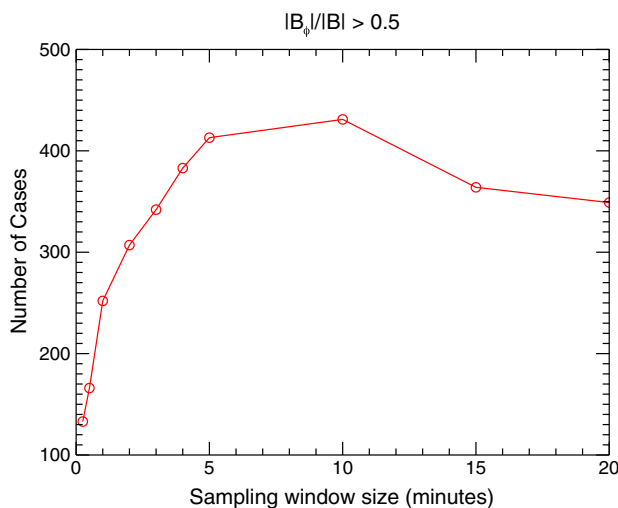
4. Data Analysis

The data analysis follows the comprehensive boundary analysis of *Delamere et al.* [2013] using Cassini Plasma Spectrometer (CAPS) [*Young et al.*, 2004] ion singles data (SNG), CAPS electron spectrometer (ELS), and the 1 min averaged Cassini magnetometer (MAG) data [*Dougherty et al.*, 2004] from 27 June 2004 to 2 June 2012. These dates include all available CAPS data. The boundary analysis identifies all magnetopause boundary crossing and bow shock crossings. Figure 3 shows the three regions encountered by the Cassini spacecraft during this time (blue=magnetosphere, red=magnetosheath, and green=solar wind) based on our boundary crossing analysis. In this paper we are only interested in identifying current sheet (CS) crossings inside of the magnetosphere (blue).

The survey included all local times and was limited to $\pm30°$ latitude to isolate encounters with the magnetodisc. The magnetic field data were given in kronian r, θ, and ϕ coordinates. The radial (B_r) and azimuthal (B_ϕ) components were used to identify current sheet crossings. The expected magnetic field topology for Saturn's magnetodisc (see Figure 1) is a southward directed normal component ($+B_\theta$) based on the dipole orientation with radial and azimuthal components changing signs depending on the location of the spacecraft with respect to the current sheet (i.e., above or below the current sheet) [*Kivelson*, 2014]. The B_r and B_ϕ components will be out of phase if the magnetic field bends back and in phase if the magnetic field bends forward.
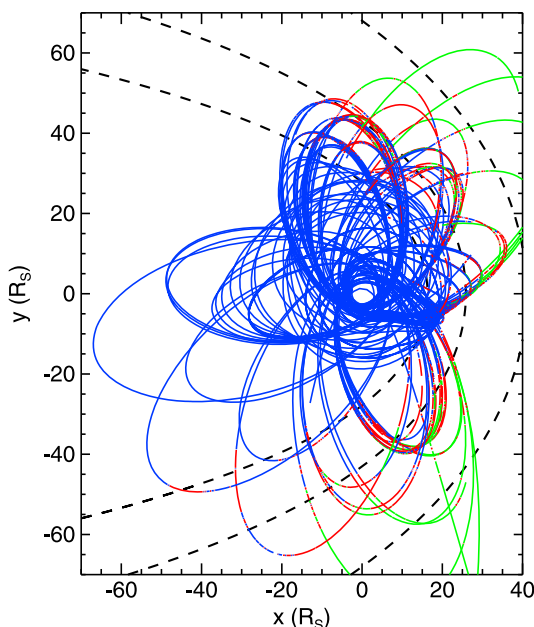
Figure 3. Saturn's boundary identification. Blue = magnetosphere, red = sheath, green = solar wind. The dashed lines are model magnetopause locations for high/inner (0.1 nPa), nominal (0.01 nPa), and low/outer (0.001 nPa) solar wind dynamic pressure [*Kanani et al.*, 2010].

Naively, one might expect the current sheet crossing to be fairly infrequent because the magnetic dipole is (roughly) aligned with the spin axis, relying instead on spacecraft motion through the magnetodisc. In this case a long time sampling window (e.g., hours) would be sufficient to identify the CS crossings. However, as we will show, the majority of consecutive CS crossings occur with a few minutes' separation and, in fact, much of the magnetodisc contains current sheets with considerable magnetic structure.

Our automated search for current sheet crossings used the following algorithm. While Cassini was within the magnetosphere, we selected a time sampling window of 5 min to identify changes in sign of both the B_r and B_ϕ components. Figure 4 is a survey of the 2007 Cassini 1 s magnetometer data for cases where $|B_\phi|/|B| > 0.5$ as a function of sampling window size. For $\Delta t < 5$ min the number of cases falls steeply as the time sample approaches kinetic spatial scales (see discussion below). Using a cross-correlation method, the phase of the sign change was determined to classify the CS crossing as bend forward or bend back. We note that the field topology cannot be uniquely determined because intense field-aligned currents will give both in-phase and out-of-phase variations in B_r and B_ϕ similar to the "camshaft" periodic magnetic signal seen between 12 and 15 R_S [*Southwood and Kivelson*, 2007]. The majority of our CS crossings were found between 20 and 30 R_S and thus largely exclude the camshaft field-aligned currents though other (e.g., auroral) field-aligned currents could contribute to our survey. We further note that angular momentum transfer to the magnetodisc from the planet requires a bend back configuration, consistent with a corotation-enforcing radial current [*Ray et al.*, 2010]. Finally, in every CS crossing we identify the minimum B_θ value in the sampling window to further constrain the thickness of the current sheet. In many cases the predominantly positive B_θ component (southward) changed signs, indicating a northward orientation. These cases are particularly interesting in the context of magnetic reconnection.

Figure 5 illustrates the time between consecutive current sheet crossings. For each CS crossing, the time is recorded to the next CS crossing (minimum 5 min based on sampling window). Clearly, the majority consecutive crossings occur on short time scales, suggesting a filamentary structure. It is difficult to quantify this result in terms of absolute spatial scale given the uncertainty in plasma flows, but if we assume that the spacecraft is stationary with respect to the magnetodisc and the plasma/field moves past the spacecraft at ~100 km/s [e.g., *Thomsen et al.*, 2010], then the distance between CS crossings separated by 5 min is 30,000 km
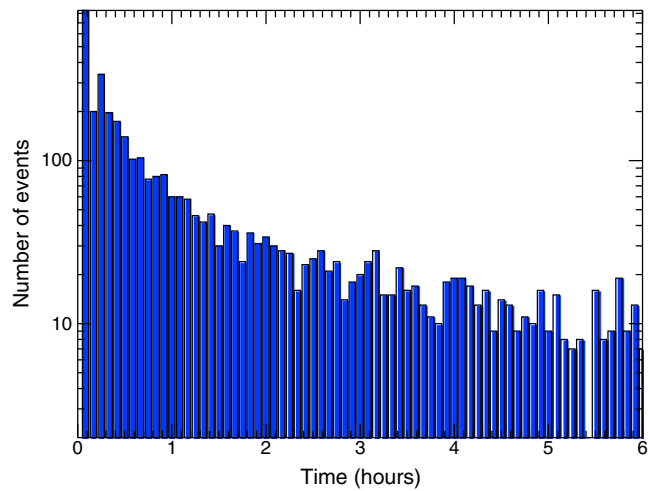

Figure 4. Survey and the 2007 Cassini 1 s magnetometer data illustrating the number of $|B_\phi|/|B| > 0.5$ cases as a function of sampling window size. The number of cases falls steeply below 5 min, demonstrating the motivation for using a 5 min window size.

Figure 5. Histogram of the time interval between consecutive current sheet crossings for all crossings, illustrating the tendency for small-scale CS structure in Saturn's magnetodisc.
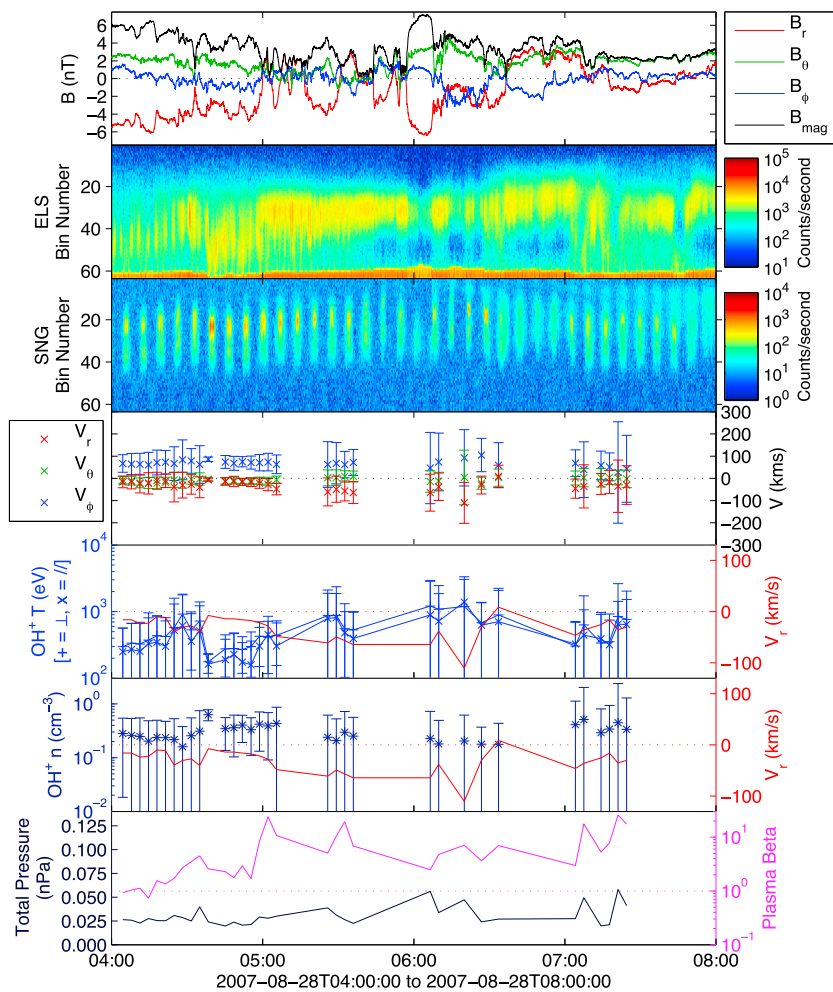
Figure 6. Example of filamentary CS crossing at Saturn. The sample 4 h interval in the premidnight sector (~20 LT, $r \sim 20\ R_S$) was taken from 28 August 2007. Numerous magnetic filaments/current sheets are seen in the first panel with $B_\theta < 0$ (green) in some instances. The second and third panels show the electron and ion data. The fourth, fifth, and sixth panels show plasma density, velocity, and temperature determined from forward fitting methods of the CAPS data. While the errors are considerable, the fits do indicate inward flows.
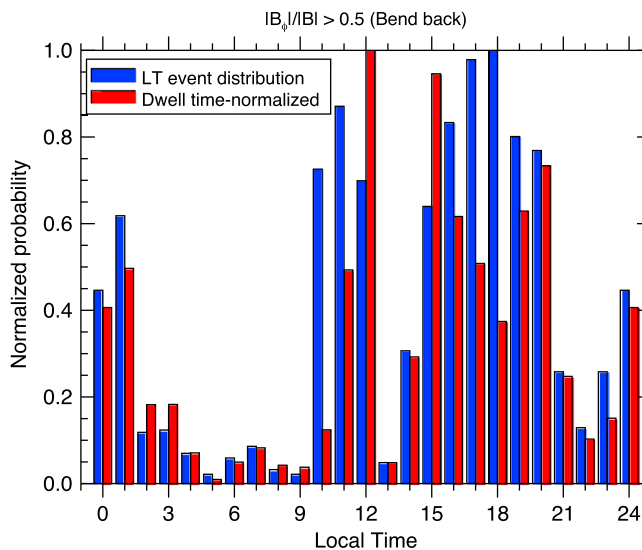
Figure 7. Local time distribution for magnetic field bend back with $|B_\phi|/|B| > 0.5$ at Saturn. Blue = raw sample, red = spacecraft dwell time normalized.

or 0.5 R_S. Using typical plasma parameters in the outer magnetosphere [e.g., *Wilson et al.*, 2012] this corresponds to ~30 ion inertial lengths (c/ω_{pi}) with each CS crossing lasting ~1 min corresponding to ~10 c/ω_{pi}. Our sampling window of 5 min specifically filters for these fragmented CS crossings.

Figure 6 shows an example interval from 28 August 2007 in the premidnight sector (~20 LT, $r \sim 20\ R_S$). We show the magnetometer data (1 s MAG) to illustrate a filamented current sheet where the red, green, and blue lines are the respective B_r, B_θ, and B_ϕ magnetic field components and the black line is the total magnetic field. At the beginning of the interval, the magnetic field is dominated by the radial component and the positive B_ϕ component is consistent with a bend back configuration ($B_r B_\phi < 0$). Gradually, the field grows weaker and $B_r B_\phi > 0$, consistent with a bend forward configuration. Between ~05:00 and 07:00, the magnetic field fluctuates with numerous current sheet encounters and occasional cases of $B_\theta < 0$. Most of the fluctuations are characterized by $B_r B_\phi < 0$, but occasional instances of $B_r B_\phi > 0$ do occur, suggesting proximity to the expected reconnection sites. These are the types of fluctuations that we have analyzed. Comparisons with plasma observations are beyond the scope of this paper, but we will conduct a comprehensive analysis of the plasma data as a future effort.

The remaining panels in Figure 6 show the CAPS electron (ELS) and ion (SNG) data, followed by plasma properties (velocity, temperature, density, and pressure) determined with forward fitting methods of the CAPS/SNG data [e.g., see *Wilson et al.*, 2012, 2013]. We first note that the CAPS/SNG actuation interval is too long to capture some of the abrupt CS crossings (~1 min); therefore, the modeled plasma properties cannot resolve filamentary structures containing possibly different plasma properties. Nevertheless, the data show corotational flows between 50 and 100 km/s along with comparable inward radial flows. This example also indicates that inward radial flows are correlated with higher temperatures and lower density (red line indicates v_r in the fifth and sixth panels), consistent with the expectation of high-temperature and low-density flux tubes originating in the outer magnetosphere. The total pressure (magnetic + plasma) is reasonably constant (i.e., ±50%) given the large errors in the plasma properties. While a dynamically evolving magnetodisc may contain some pressure imbalance, the expectation for local pressure balance provides a good indication of the reliability of the forward model fits. The plasma β also increases during this interval as expected for conditions near the center of the magnetodisc. More detailed comparisons with plasma observations are beyond the scope of this paper, but we will conduct a comprehensive analysis of the plasma data as a future effort.

To quantify the relative thickness of the current sheets and proximity to a potential X-line, we use the ratio $|B_\phi|/|B| > 0.5$, where the time sampling of 5 min further filters for kinetic scales as discussed above. Using the bend back criterion, Figure 7 shows the local time distribution of these potentially critically thin current sheets. The blue histogram is the normalized sampling of the CS crossings, and the red histogram is spacecraft "dwell" time normalized to filter for nonuniform local time sampling. The majority of the CS crossings occur
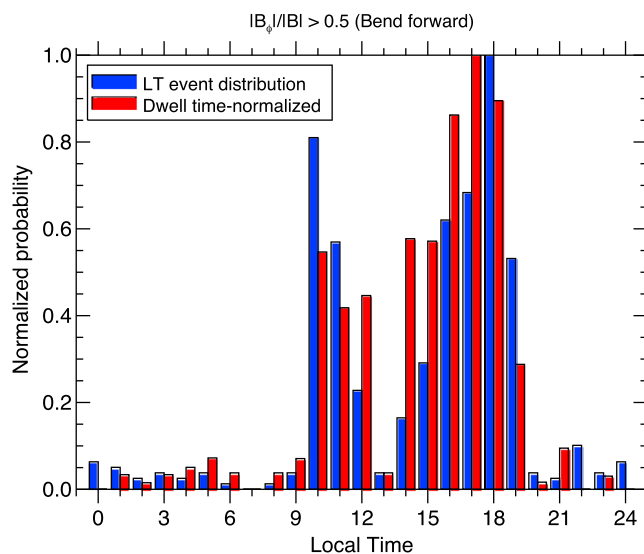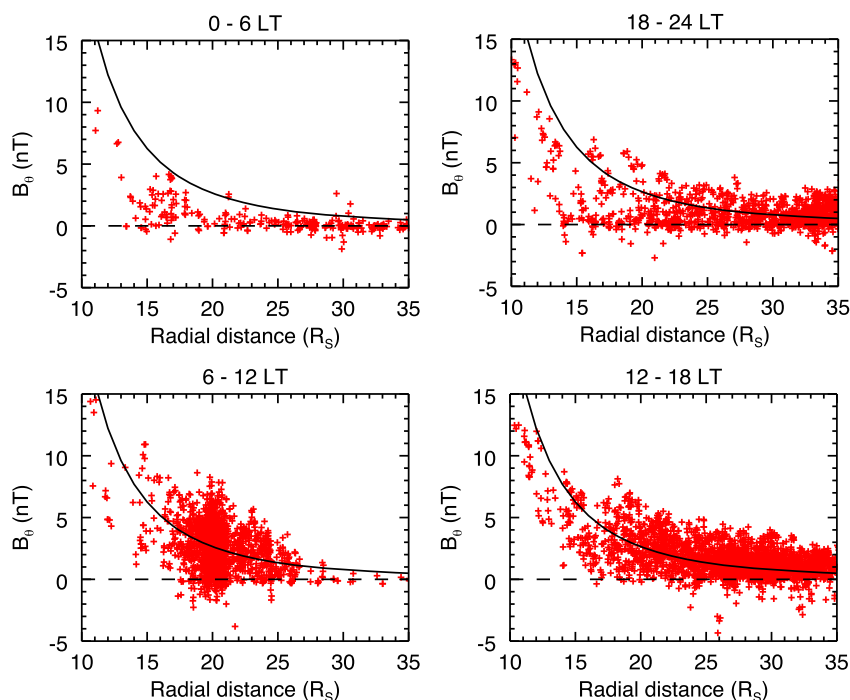
Figure 8. Local time distribution for magnetic field bend forward with $|B_\phi|/|B| > 0.5$ at Saturn. Blue = raw sample, red = spacecraft dwell time normalized.

in the subsolar and dusk sector with a few events occurring in the midnight tail sector. Many of the tail events have been identified by *Jackman et al.* [2014] and are assumed to be associated with tail reconnection. The gap at 13:00 LT is assumed to be related to the set of high-latitude Cassini orbits; therefore, sampling of this local time sector at low latitude is sparse. Figure 8 is the same as Figure 7 but for the bend forward criterion, showing nearly all cases in the subsolar to dusk sector.

The normal magnetic field component, B_θ, is expected to remain southward ($B_\theta > 0$) inside of the magnetosphere. But in the case that magnetic reconnection is operating within the magnetodisc, $B_\theta < 0$ cases may occur. Figure 9 summarizes the LT distribution of the B_θ component in the sampling window.

The black line is the dipole field. In the 0–6 LT sector, the CS is uniformly thin with values of B_θ less than the dipole. In the prenoon sector (6–12 LT), the distribution of B_θ varies from negative to larger than the dipole field. The postnoon sector (12–18 LT) shows a distribution scattered about the dipole with a somewhat uniform spread of values. The premidnight sector shows a combination of thin current sheet and dipole-like values, indicating variable conditions. There are negative B_θ values in every local time sector. Figure 10 shows the local time distribution of the $B_\theta < 0$ events with the dwell time normalization. Interestingly, a large number of cases occur in the subsolar to dusk sector and appear more frequently than the tail cases.

Figure 9. Minimum B_θ for all Saturn current sheet crossings in local time sectors. The black line is the planetary dipole B_θ component in the equatorial plane.
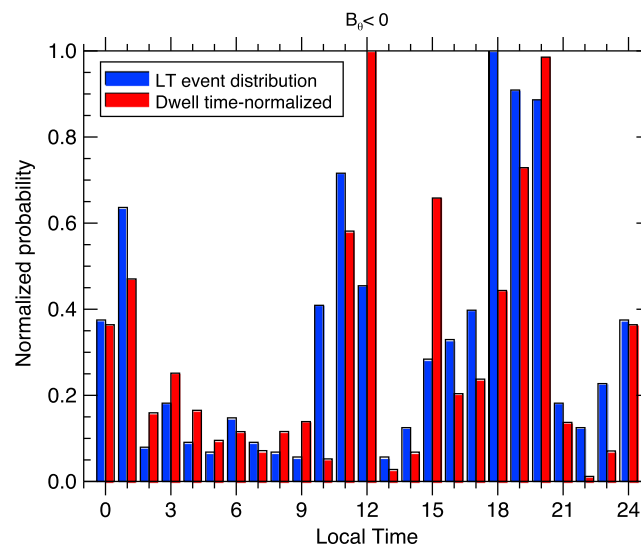
Figure 10. Local time distribution for $B_\theta < 0$ for Saturn current sheet crossings. Blue = raw sample, red = spacecraft dwell time normalized.

Finally, we examined the radial distribution of all current sheet crossings for the four cases summarized in Table 1. In all cases we fit a Gaussian to the radial distribution to quantify the peak and the width (full width at half maximum (FWHM)) of the distribution. The $B_\theta > 0$ cases both peak at smaller radial distances compared with the $B_\theta < 0$ cases, consistent with the expectation for an X-line configuration (e.g., see X-line in Figure 2). While likely not statistically significant, we note that the bend forward $B_\theta > 0$ case (Case 1) has the smallest peak radial distance, consistent with our expectation for inward moving, low-entropy flux tubes. If the bend forward $B_\theta > 0$ peak occurred at a larger radial distance than the bend back $B_\theta > 0$ peak, then solar wind stresses near the magnetopause boundary could potentially account for this observation. The majority of the bend back $B_\theta > 0$ cases (Case 2) represent likely events of mass loaded thinning current sheets that have not yet experienced reconnection. Unless $B_\theta < 0$ is caused by a projection effect of a strongly bent flux tube, we expect that Cases 3 and 4 represent plasmoid encounters which must involve reconnection. This expectation is supported by the fact that the radial distributions are different for the $B_\theta < 0$ and the $B_\theta > 0$ cases. For instance, the peaks of the $B_\theta < 0$ cases are at greater radial distances, which is consistent with the rapid outward motion of these plasmoids due to the abruptly dominant centrifugal stresses following reconnection. Since the leading portion of plasmoids has $B_\theta > 0$, we expect that the number of plasmoid encounters with $B_\theta > 0$ be similar to the total of all $B_\theta < 0$ events. We note that overall azimuthal distributions (Figures 6 and 7) do not change significantly for the plasmoid subset of all $B_\theta > 0$ cases.

5. Discussion

5.1. Conceptual Model for Magnetic Flux Circulation

Figure 1 summarizes our conceptual model for flux circulation in the giant magnetospheres. The model applies to the middle and outer magnetospheres where radial plasma transport is assumed to be tied to magnetic reconnection and current sheet collapse. The tailward flows in the nightside magnetosphere are based on an analysis of plasma data from the Cassini CAPS [*Thomsen et al.*, 2014] and Ion Neutral Camera [*Kane et al.*, 2014] instruments, showing respectively a "planetary wind" along the dusk flank and a "low-latitude bound-

Table 1. Radial Distribution of All CS Crossings at Saturn

Case	B_θ	Bend	Peak (R_S)	FWHM (R_S)	Number of Events
1	+	forward	24.64	9.34	2851
2	+	back	25.51	8.64	4527
3	−	forward	34.23[a]	8.00	229
4	−	back	27.23	8.21	607

[a]Gaussian fit, not dwell time normalized.

ary layer" along the dawn flank. Following *Mitchell* [2015], we distinguish this type of transport from flux tube interchange that likely occurs in the inner magnetosphere on dipole magnetic field lines. The mass transport processes must remove mass from the magnetosphere; therefore, net mass transport can be viewed as an outward process with transport rate $\dot{M}$. Magnetic flux transport, on the other hand, must be a two-way process so that planetary magnetic flux is conserved. Using simple mass conservation principles, *Delamere and Bagenal* [2010] and *Bagenal and Delamere* [2011] showed that a parcel of plasma is transported rapidly outward from the middle magnetosphere to the tail within a final "lap of honor." The rapid plasma outflow must be accompanied by a rapid inflow of empty flux tubes returning magnetic flux.

Our analysis of the current sheet crossings shows that most of the encounters occur in the subsolar to dusk sector with a smaller distribution of events in the midnight sector where tail reconnection is expected to occur. We propose that reconnection is operating primarily on *closed* field lines starting deep in the closed field line region in a complex and patchy network of reconnection sites. The frequency of CS encounters, the large variation in the magnitude of B_θ, and the frequent occurrence of negative B_θ are impossible to reconcile with large-scale (many R_S) transport. Therefore, these observations suggest significant small-scale structure (e.g., $< 1R_S$) for the returning flux channels. We use the term "reconnection drizzle" to imply the concept of patchy reconnection as opposed to a global-scale (i.e., many R_S) X-line. The dusk flank is likely a composite of plasma blobs that are both magnetically coupled and decoupled to the planet, ultimately moving into the tail. These plasma blobs can be considered similar to the bubbles of plasma described by *Kivelson and Southwood* [2005] moving down Jupiter's dusk flank that have broken off the outer edge of the magnetodisc. In Figure 1 we illustrate this region of the outer magnetosphere with complex magnetic topology in the form of detached plasmoids.

A bend forward configuration is not expected with plasma outflow. Yet we find many bend forward cases in the subsolar and dusk sector. One possibility is that tailward viscous stresses exerted by the solar wind at the magnetopause boundary bends the field tailward/forward. However, these cases should only occur close to the magnetopause boundary. The prevalence of bend forward cases at all radial distances from middle to outer magnetosphere suggest that the solar wind is not completely responsible. Also, the subsolar cases cannot be caused by solar wind stresses. We propose, instead, that these cases result from the inward motion of low-entropy flux tubes generated by reconnection, where conservation of angular momentum increases the angular velocity and generates the bend forward flux tubes. In Figure 1, we show the dusk magnetic field in a bend forward configuration.

Plasmoids are likely to develop first in a bend back configuration because reconnection is expected for mass loaded, stretched flux tubes with a strong bend back. The bend forward $B_\theta < 0$ cases (Case 3) may be related to a twisting of the plasmoid due to a difference in the azimuthal speed of the outer and inner edges of the plasmoid. This difference can arise if a plasmoid contracts, the inner edge moves rapidly outward, and via angular momentum conservation, slows relative to the outer edge. It is not clear how these plasmoids are assimilated in the outer magnetosphere before being ejected down the tail, but they are consistent with Voyager observations of detached plasma in Saturn's dayside magnetosphere by *Goertz* [1983].

It is important to note that the expected time scales of these reconnection processes are well below the coupling time for ionospheric feedback; therefore, ionospheric feedback cannot be considered in a simple steady state coupling model. Rather, it is expected that returning Alfvénic signatures from the ionosphere arrive well after a magnetodisc reconnection event and possibly contribute to the very dynamic magnetic configuration of the magnetodisc.

This model does not provide a physical explanation for the observed local time dependence, but clearly, the solar wind interaction must be a fundamental driver of the flux circulation pattern. In the context of the Vasyliunas cycle, we argue that the model of a single X-line in the tail is an oversimplification, but the net effect of distributed and/or patchy reconnection through the dusk sector accomplishes the same task of releasing plasma down the dusk flank.

5.2. The Magnetic Cushion Region

A key aspect of our conceptual model is the presence of a magnetic cushion. The cushion is defined as a reservoir of magnetic flux (exceeding the dipole field strength) between the current sheet and the magnetopause boundary (the terminology was first proposed by V. M. Vasyliunas in 1992). At Jupiter, the cushion region is a well-defined region [e.g., *Kivelson and Southwood*, 2005], while at Saturn the presence of a cushion is not clear
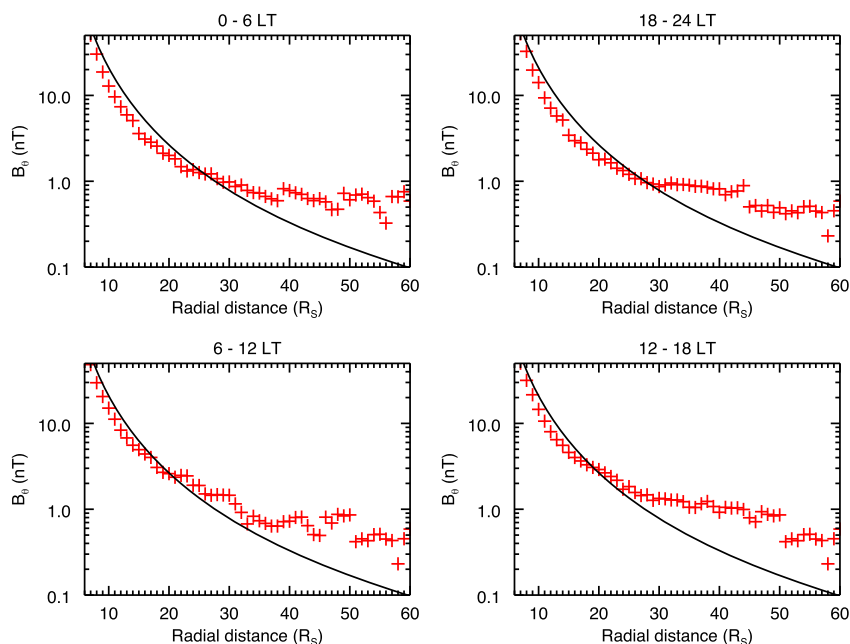
Figure 11. Radial averages of B_θ for four local time sectors illustrating the flux deficit in Saturn's inner magnetosphere ($< 20-25\ R_S$) and the flux surplus (cushion) in the outer magnetosphere. The black line is the planetary dipole B_θ component in the equatorial plane.

[*Went et al.*, 2011]. We argue that the cushion is a necessary consequence of the magnetodisc formation and is the accumulation of expelled flux from the current sheet. *Arridge et al.* [2008] noted that magnetodisc formation (i.e., when the centrifugal stress dominates mechanical stress) occurs during low solar wind dynamic pressure, but under compression the magnetodisc is only present on the nightside and flanks of the magnetosphere. The cushion is a general result in any 2-D equilibrium for the giant-planet magnetodiscs [e.g. *Caudal*, 1986; *Chou and Cheng*, 2010]. In equilibrium, the flux deficit (measured as a difference from the dipole field) is balanced by the flux surplus in the outer magnetosphere.

We have adopted two methods for quantifying the flux contained in Saturn's magnetic cushion. The first method uses 1 h averages of the Cassini MAG data for low latitudes (i.e., $\pm 30°$ latitude) and determines the flux surplus/deficit with respect to the dipole field at all spacecraft locations. The results of this survey are shown in Figure 11 for four local time sectors where averages in each 1 R_S radial bin are plotted (red). The dipole is shown as the black line. The total deficit is 18.3 GWb, and the total surplus (cushion) is 18.5 GWb, showing that on average flux is conserved despite the limited radial coverage in the tail region. This estimate is likely an underestimate since the cushion coverage is incomplete, and the flux deficit is contaminated by field lines in the inner magnetosphere mapping out to the cushion region.

The second method measures the flux at each current sheet crossing, computing averages per radial bin in each local time sector. At each current sheet crossing the minimum B_θ is found in the sliding window and recorded as a difference from the magnetic dipole. If $B_\theta > 0$, then the current sheet crossing is assumed to be planetward of any possible X-line, while for $B_\theta < 0$ the current sheet crossing is assumed to be located radially outward from a definite X-line with field lines mapping into the cushion region. Flux averages are calculated for each case of positive and negative B_θ and in each radial bin. For a survey of current sheet crossing between 6 and 40 R_S, the $B_\theta > 0$ flux deficit was 29 GWb, and for the $B_\theta < 0$ cases, the flux surplus (cushion) was 30 GWb. We consider this as the most accurate estimate of the cushion flux, and as expected the cushion flux is larger than the method 1 estimate of ~18 GWb. If we expand the survey beyond 40 R_S, the cushion flux increases (e.g., 36 GWb at 50 R_S), but this is likely due to errors from open and tangled flux in the tail.

5.3. Flux Transport and Reconnection Potential
Radial flux transport can be estimated empirically following *Bagenal and Delamere* [2011]. A radial mass outflow rate ~60 kg/s has been determined using physical chemistry models of the partially ionized plasmas in
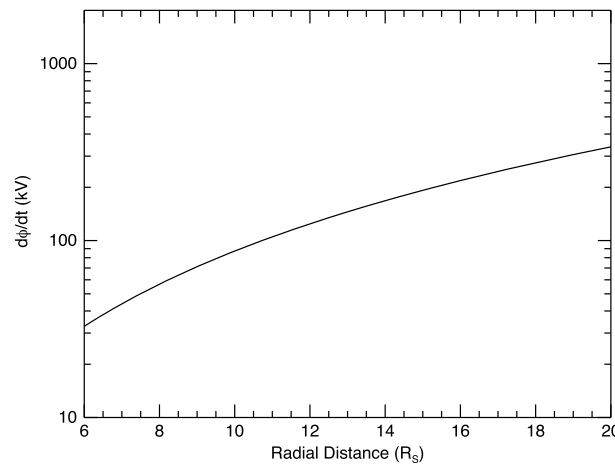
Figure 12. Empirical flux transport potential for radial mass outflow at Saturn given by *Bagenal and Delamere* [2011] inside of 20 R_S.

Saturn's inner magnetosphere by *Fleshman et al.* [2013]. The radial mass transport rate from conservation of mass is

$$\dot{M} = 2\pi r H u_r m n \qquad (2)$$

where R is radial distance from Saturn, H is the scale height of the plasma torus, m is the average ion mass, and n is the density. Beyond $r \approx 8\ R_S$, the radial mass outflow is constant; therefore, the radial outflow speed can be determined as a function of radial distance using empirical values for H and n. Given u_r, the magnetic flux transport rate is

$$\frac{d\phi}{dt} = 2\pi r (u_r B_\theta) \qquad (3)$$

where B_θ is the dipole field. Figure 12 shows an estimate of the magnetic flux transport rate inside of 20 R_S, where the maximum potential at 20 R_S is ~300 kV. We do not carry this estimate outside of 20 R_s because the empirical profiles for n and H from *Bagenal and Delamere* [2011] are only available to 20 R_S. The potentials could be higher at larger radial distances.

We estimate the outward flux transport time scale by numerically solving a one-dimensional flux conservative equation for magnetic flux transport of the form $\partial_t \phi + \partial_r (u_r \phi) = 0$, where r is radial distance. Note that the steady state solution requires the return of magnetic flux that is not considered here. The initial flux is from the dipole field, ϕ_{DP}, and we use the empirical inputs from *Bagenal and Delamere* [2011] extrapolated to 40 R_S and equations (2) and (3) to determine the radial outflow. The inner boundary is fixed with ϕ_{DP}, and the outer boundary is open (i.e., $\partial_r = 0$). The respective time scales for the transport of 18 GWb and 29 GWb of flux out of the inner and middle magnetosphere (i.e., $\phi_{DP} - \phi$ between 5 and 25 R_S) is ~25 h and ~70 h. *Rymer et al.* [2013] estimated the time scale for Saturn's magnetospheric refresh rates following the current sheet stress balance considerations of *Kronberg et al.* [2007] and found a time scale of 30.7 h for $\dot{M} = 56.9$ kg/s, consistent with our estimate. While our model does not support large-scale plasmoid release down the magnetotail as the dominant mechanism for flux circulation, observable magnetospheric quasiperiodicities should be coupled to flux circulation time scales. For example, large-scale magnetospheric reconfiguration following solar wind compressions that trigger tail reconnection should be characterized by a ~30 h magnetospheric refilling period. While large-scale plasmoids may be present in the tail, modulated by the refresh rate, the dominant plasma loss mechanism can remain small-scale "drizzle".

Quasi-steady flux transport requires equivalent magnetic reconnection potentials (i.e., hundreds of kilovolts), allowing flux to return to the inner magnetosphere. *Jackman et al.* [2014] estimated that 0.26–2.2 GWb of flux was closed during a 27 min postplasmoid plasma sheet encounter of the Cassini spacecraft. The range of values is dependent on the assumption of azimuthal extent of the X-line (with the upper limit corresponding to the full tail width of 90 R_S) and the flow speed of the plasmoid. The corresponding reconnection voltages are 160–1330 kV and are consistent with our estimates for closed magnetic flux transport. We note that reconnection potentials ~300 kV are significantly larger than the inferred dayside opening reconnection potentials given by *Masters et al.* [2014] (i.e., 10–70 kV). Therefore, magnetodisc and magnetotail reconnection should predominantly operate on closed magnetic field lines enabling the inward transport of magnetic flux. The amount of open flux that is required to be reclosed is small compared to the closed flux that is transported outward with mass. An individual reconnection process may possibly reconnect open field lines as a secondary consequence provided that local conditions are suitable. However, the large reconnection potentials are consistent with mandatory closed flux circulation, and therefore, it is unlikely the Dungey cycle can be considered as a primary driver of magnetospheric dynamics. A similar situation exists at Jupiter where the flux circulation potential for $\dot{M} = 500$ kg/s and for the empirical inputs from *Bagenal and Delamere* [2011] is ~10 MV, dominating the dayside reconnection potential (e.g., ~100–1000 keV) [*Nichols et al.*, 2006].

5.4. Auroral Implications

Jupiter's and Saturn's aurora are complex structures, driven by a variety of mechanisms. *Grodent* [2014] reviewed the morphologies of ultraviolet auroral emissions of these gas giants, attempting to capture the diversity of emission features in a single sketch that single images fail to capture. Despite this complexity, there is abundant literature published that attempts to use the gross auroral structure to identify the open/closed magnetic field line boundary. In the discussion that follows we assume that all auroral emissions occur on closed field lines and that the flux content of the open polar cap cannot necessarily be delineated by auroral emissions. Our suggestions for the location of the open/closed boundary are consistent with our conceptual model but may stand in stark contrast to other published literature on the topic.

Two limiting cases can be used to understand the solar wind interaction at Jupiter and Saturn. The first is the Dungey cycle of large-scale magnetic reconnection, and the second is a viscous interaction that can involve intermittent small-scale reconnection that may have little impact on the open flux content of the polar cap [*Delamere*, 2015]. The former is used quite successfully at Earth but has been questioned as a primary driver of magnetospheric dynamics at the giant magnetospheres [*Delamere and Bagenal*, 2010; *Masters et al.*, 2014]. The amount of open flux in the polar cap is a critical measure of the Dungey cycle as net flux transport can take place into or out of the magnetosphere, enlarging or shrinking the size of the polar cap. Earth's aurorally dark polar cap makes using the main oval of emissions a reasonable proxy for the open/closed boundary, with auroral emissions occurring on closed field lines. Jupiter's aurorally active polar region renders an unambiguous identification of the open/closed boundary impossible. Saturn, on the other hand, has an Earth-like dark polar region, and the auroral emissions have been used to identify the open/closed boundary in several studies [e.g., *Badman et al.*, 2005; *Radioti et al.*, 2011; *Badman et al.*, 2014]. In this discussion, we leverage the Cassini CS observations and the auroral observations to describe a model for flux circulation that is similar for Jupiter and Saturn, but distinctly different from Earth.

Although the the auroral oval is a good proxi for Earth's open polar cap, the most magnificent auroral displays are associated with substorms that start well inside of the closed magnetic field region. Likewise, we expect magnetic flux transport and magnetodisc reconnection to be associated with significant auroral signatures similar to those described by *Radioti et al.* [2013] in the subsolar and postnoon sector. These signatures should be deep inside the closed magnetosphere with the equatorward edge probably close to the transition from dipolar to stretched magnetodisc magnetic field. A second reference for magnetodisc-driven aurorae is provided by the cushion region where strong shear and the presence of entangled magnetic field provide a source for auroral signatures. Since the cushion is on closed field lines, any aurora close to the poleward edge should be considered as a proxi for the outer or poleward boundary of the closed magnetic field region.

The dark polar region (DPR) [*Stallard et al.*, 2003] poleward of Jupiter's dawn main emissions have been shown to be partially on closed field lines [*Vogt et al.*, 2011]. If the cushion region and closed flux along the dawn flank are included, then much of the DPR is likely on closed field lines. If Saturn also has a cushion region, then portions of the aurorally dark polar region would be on closed field lines. This is an important consideration given the recent observations of bifurcations in Saturn's aurora in the subsolar and dusk sector [*Radioti et al.*, 2011; *Badman et al.*, 2013] (see Figure 13). We argue that these auroral forms (starting at high latitude and merging with the main emissions at lower latitude) are not caused by enhanced dayside magnetopause reconnection but rather are generated by larger events of enhanced radial inflows required for magnetic flux circulation. Similar bifurcations are seen at Jupiter with multiple arcs found in the dusk sector. Figure 13 summarizes our alternative explanation for these auroral forms. In both cases we identify an open/closed boundary (dotted circle), a dawn cushion region (aurorally dark), and the subsolar to dusk bifurcations associated with return magnetic flux channels.

We note that the upper limit for the flux content of Saturn's polar cap was estimated to be ≤ 20 GWb by *Delamere* [2015], where the planetary dipole field was integrated from the magnetopause subsolar distance ($\sim 22 R_S$) to infinity to determine this upper limit. This is qualitatively consistent with the dotted circle region shown in Figure 13 at 10° co-latitude, where *Radioti et al.* [2011] estimated the open flux to be 20–30 GWb using the auroral emissions to define the open/closed boundary. We also note that 10° co-latitude was the lower limit for the northern polar cap boundary determined by *Jinks et al.* [2014] with a multi-instrument assessment.

The aurorally dark dawn sector, composed of the cushion region and thin current sheet, is consistent with the general lack of CS encounters with $|B_\phi|/|B| > 0.5$. While the overall current sheet might be considered thin
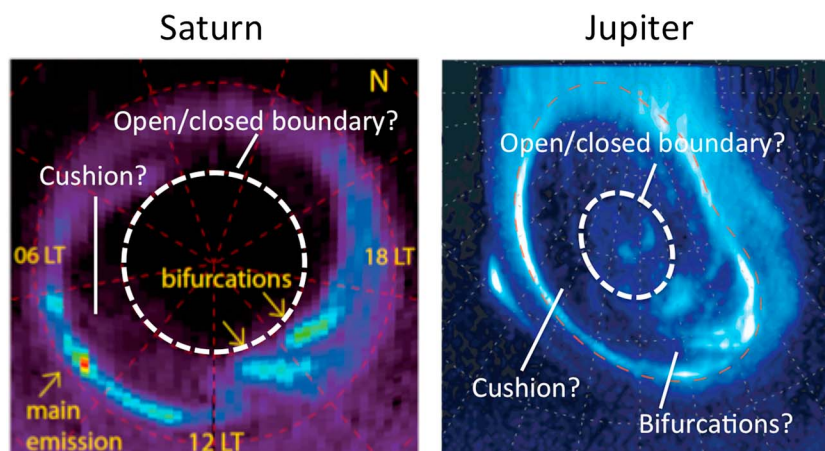
Figure 13. Proposed analogy for Jupiter's and Saturn's aurora, illustrating the dawn signature of a cushion region (aurorally dark), subsolar to dusk sector bifurcations, and the possible location of the open/closed field line boundary (dotted circle). Saturn's auroral image was taken with the Cassini Ultraviolet Imaging Spectrograph instrument [*Radioti et al.*, 2011], and Jupiter's northern UV auroral image was taken from the Hubble Space Telescope [*Nichols et al.*, 2007].

in this sector, magnetic reconnection is not operating frequently. It follows that auroral emissions are likely triggered by magnetic flux inflows that rarely occur in this sector.

6. Conclusions

We present a comprehensive analysis of current sheet crossing in Saturn's magnetosphere in an attempt to understand the two-way magnetic flux transport in the rapidly rotating giant magnetospheres. We summarize our findings as follows:

1. Magnetic reconnection occurring on closed field lines mapping to a magnetic cushion region within the magnetodisc may be a critical component of magnetic flux circulation through the generation of low-entropy flux tubes in the outer magnetosphere.
2. The presented observations of frequent current sheet crossing, large B_θ variations, and frequent negative B_θ observations are inconsistent with large-scale inward plasma transport and large-scale reconnection events, supporting the idea that plasma can be lost on small scales through a "drizzle"-like process.
3. Surprisingly, many current sheet crossings and potential reconnection sites are found in the subsolar and dusk sector, suggesting that reconnection in this sector can play a significant role in addition to tail reconnection (Figures 7 and 8).
4. Our conceptual model (Figure 1) of magnetic flux circulation augments the original Vasyliunas cycle, implying that much of the required reconnection occurs in a complex and patchy network of reconnection sites that ultimately allows plasma to exit primarily on the dusk flank.
5. Tail reconnection forms the infrequently observed nightside plasmoids and facilitates plasma loss on the dawn flank.
6. Reconnection potentials ∼300 kV associated with closed flux circulation support the argument that the Dungey cycle is a secondary driver of magnetospheric dynamics.
7. Comparisons of Jupiter's and Saturn's aurora (Figure 13) suggest that inward flux transport generates auroral emissions on closed field lines and that the open/closed boundary is not unambiguously defined by auroral emissions (i.e., dark regions in the polar region may lie on closed field lines).

References

Achilleos, N., P. Guio, and C. S. Arridge (2010), A model of force balance in Saturn's magnetodisc, *Mon. Not. R. Astron. Soc.*, *401*, 2349–2371, doi:10.1111/j.1365-2966.2009.15865.x.

Arridge, C. S., C. T. Russell, K. K. Khurana, N. Achilleos, S. W. H. Cowley, M. K. Dougherty, D. J. Southwood, and E. J. Bunce (2008), Saturn's magnetodisc current sheet, *J. Geophys. Res.*, *113*, A04214, doi:10.1029/2007JA012540.

Badman, S. V., E. J. Bunce, J. T. Clarke, S. W. H. Cowley, J.-C. Gérard, D. Grodent, and S. E. Milan (2005), Open flux estimates in Saturn's magnetosphere during the January 2004 Cassini-HST campaign, and implications for reconnection rates, *J. Geophys. Res.*, *110*, A11216, doi:10.1029/2005JA011240.

Badman, S. V., A. Masters, H. Hasegawa, M. Fujimoto, A. Radioti, D. Grodent, N. Sergis, M. K. Dougherty, and A. J. Coates (2013), Bursty magnetic reconnection at Saturn's magnetopause, *Geophys. Res. Lett.*, *40*, 1027–1031, doi:10.1002/grl.50199.

Badman, S. V., C. M. Jackman, J. D. Nichols, J. T. Clarke, and J.-C. Gérard (2014), Open flux in Saturn's magnetosphere, *Icarus*, *231*, 137–145, doi:10.1016/j.icarus.2013.12.004.

Bagenal, F. (2007), The magnetosphere of Jupiter: Coupling the equator to the poles, *J. Atmos. Sol. Terr. Phys.*, *69*, 387–402, doi:10.1016/j.jastp.2006.08.012.

Bagenal, F., and P. A. Delamere (2011), Flow of mass and energy in the magnetospheres of Jupiter and Saturn, *J. Geophys. Res.*, *116*, A05209, doi:10.1029/2010JA016294.

Birn, J., R. Nakamura, E. V. Panov, and M. Hesse (2011), Bursty bulk flows and dipolarization in MHD simulations of magnetotail reconnection, *J. Geophys. Res.*, *116*, A01210, doi:10.1029/2010JA016083.

Caudal, G. (1986), A self-consistent model of Jupiter's magnetodisc including the effects of centrifugal force and pressure, *J. Geophys. Res.*, *91*, 4201–4221, doi:10.1029/JA091iA04p04201.

Chou, M., and C. Z. Cheng (2010), Modeling of Saturn's magnetosphere during Voyager 1 and Voyager 2 encounters, *J. Geophys. Res.*, *115*, A08202, doi:10.1029/2009JA015124.

Delamere, P. A. (2015), *Magnetotails in the Solar System*, chap. Solar wind interaction with the giant magnetospheres and Earth's magnetosphere, John Wiley, Hoboken, N. J.

Delamere, P. A., and F. Bagenal (2010), Solar wind interaction with Jupiter's magnetosphere, *J. Geophys. Res.*, *115*, A10201, doi:10.1029/2010JA015347.

Delamere, P. A., R. J. Wilson, S. Eriksson, and F. Bagenal (2013), Magnetic signatures of Kelvin-Helmholtz vortices on Saturn's magnetopause: Global survey, *J. Geophys. Res. Space Physics*, *118*, 393–404, doi:10.1029/2012JA018197.

Delamere, P. A., F. Bagenal, C. Paranicas, A. Masters, A. Radioti, B. Bonfond, L. Ray, X. Jia, J. Nichols, and C. Arridge (2014), Solar wind and internally driven dynamics: Influences on magnetodiscs and auroral responses, *Space. Sci. Rev.*, *187*, 51–97, doi:10.1007/s11214-014-0075-1.

Dougherty, M. K., et al. (2004), The Cassini magnetic field investigation, *Space Sci. Rev.*, *114*, 331–383, doi:10.1007/s11214-004-1432-2.

Fleshman, B. L., P. A. Delamere, F. Bagenal, and T. Cassidy (2013), A 1-D model of physical chemistry in Saturn's inner magnetosphere, *J. Geophys. Res. Planets*, *118*, 1567–1581, doi:10.1002/jgre.20106.

Goertz, C. K. (1983), Detached plasma in Saturn's front side magnetosphere, *Geophys. Res. Lett.*, *10*, 455–458, doi:10.1029/GL010i006p00455.

Gold, T. (1959), Motions in the magnetosphere of the Earth, *J. Geophys. Res.*, *64*, 1219–1224, doi:10.1029/JZ064i009p01219.

Grodent, D. (2014), A brief review of ultraviolet auroral emissions on giant planets, *Space Sci. Rev.*, *187*, 23–50, doi:10.1007/s11214-014-0052-8.

Hill, T. W. (1979), Inertial limit on corotation, *J. Geophys. Res.*, *84*, 6554–6558.

Hill, T. W., et al. (2008), Plasmoids in Saturn's magnetotail, *J. Geophys. Res.*, *113*, A01214, doi:10.1029/2007JA012626.

Hsieh, M.-S., and A. Otto (2014), The influence of magnetic flux depletion on the magnetotail and auroral morphology during the substorm growth phase, *J. Geophys. Res. Space Physics*, *119*, 3430–3443, doi:10.1002/2013JA019459.

Jackman, C. M., et al. (2014), Saturn's dynamic magnetotail: A comprehensive magnetic field and plasma survey of plasmoids and traveling compression regions and their role in global magnetospheric dynamics, *J. Geophys. Res. Space Physics*, *119*, 5465–5494, doi:10.1002/2013JA019388.

Jinks, S. L., et al. (2014), Cassini multi-instrument assessment of Saturn's polar cap boundary, *J. Geophys. Res. Space Physics*, *119*, 8161–8177, doi:10.1002/2014JA020367.

Kanani, S. J., et al. (2010), A new form of Saturn's magnetopause using a dynamic pressure balance model, based on in situ, multi-instrument Cassini measurements, *J. Geophys. Res.*, *115*, A06207, doi:10.1029/2009JA014262.

Kane, M., D. G. Mitchell, J. F. Carbary, and S. M. Krimigis (2014), Plasma convection in the nightside magnetosphere of Saturn determined from energetic ion anisotropies, *Planet. Space Sci.*, *91*, 1–13, doi:10.1016/j.pss.2013.10.001.

Kasahara, S., E. A. Kronberg, T. Kimura, C. Tao, S. V. Badman, A. Masters, A. Retinò, N. Krupp, and M. Fujimoto (2013), Asymmetric distribution of reconnection jet fronts in the Jovian nightside magnetosphere, *J. Geophys. Res. Space Physics*, *118*, 375–384, doi:10.1029/2012JA018130.

Kellett, S., C. S. Arridge, E. J. Bunce, A. J. Coates, S. W. H. Cowley, M. K. Dougherty, A. M. Persoon, N. Sergis, and R. J. Wilson (2011), Saturn's ring current: Local time dependence and temporal variability, *J. Geophys. Res.*, *116*, A05220, doi:10.1029/2010JA016216.

Khurana, K. K. (2001), Influence of solar wind on Jupiter's magnetosphere deduced from currents in the equatorial plane, *J. Geophys. Res.*, *106*, 25,999–26,016, doi:10.1029/2000JA000352.

Kivelson, M. G. (2014), Planetary magnetodiscs: Some unanswered questions, *Space Sci. Rev.*, *187*, 5–21, doi:10.1007/s11214-014-0046-6.

Kivelson, M. G., and D. J. Southwood (2005), Dynamical consequences of two modes of centrifugal instability in Jupiter's outer magnetosphere, *J. Geophys. Res.*, *110*, A12209, doi:10.1029/2005JA011176.

Kronberg, E. A., J. Woch, N. Krupp, A. Lagg, K. K. Khurana, and K. Glassmeier (2005), Mass release at Jupiter: Substorm-like processes in the Jovian magnetotail, *J. Geophys. Res.*, *110*, A03211, doi:10.1029/2004JA010777.

Kronberg, E. A., K. Glassmeier, J. Woch, N. Krupp, A. Lagg, and M. K. Dougherty (2007), A possible intrinsic mechanism for the quasi-periodic dynamics of the Jovian magnetosphere, *J. Geophys. Res.*, *112*, A05203, doi:10.1029/2006JA011994.

Masters, A., M. Fujimoto, H. Hasegawa, C. T. Russell, A. J. Coates, and M. K. Dougherty (2014), Can magnetopause reconnection drive Saturn's magnetosphere?, *Geophys. Res. Lett.*, *41*, 1862–1868, doi:10.1002/2014GL059288.

Mauk, B. H., D. G. Mitchell, R. W. McEntire, C. P. Paranicas, E. C. Roelof, D. J. Williams, S. M. Krimigis, and A. Lagg (2004), Energetic ion characteristics and neutral gas interactions in Jupiter's magnetosphere, *J. Geophys. Res.*, *109*, A09S12, doi:10.1029/2003JA010270.

Mauk, B. H., et al. (2009), *Saturn from Cassini-Huygens*, chap. Fundamental plasma processes in Saturn's magnetosphere, 281 pp., Springer, Dortrecht, Netherlands, doi:10.1007/978-1-4020-9217-6-11.

Mitchell, D. G. (2015), *Magnetotails in the Solar System*, chap. Injection, interchange and reconnection: Energetic particle observations in Saturn's magnetotail, John Wiley, Hoboken, N. J.

Nichols, J. D., S. W. H. Cowley, and D. J. McComas (2006), Magnetopause reconnection rate estimates for Jupiter's magnetosphere based on interplanetary measurements at ∼5AU, *Ann. Geophys.*, *24*, 393–406, doi:10.5194/angeo-24-393-2006.

Nichols, J. D., E. J. Bunce, J. T. Clarke, S. W. H. Cowley, J. C. Gérard, D. Grodent, and W. R. Pryor (2007), Response of Jupiter's UV auroras to interplanetary conditions as observed by the Hubble Space Telescope during the Cassini flyby campaign, *J. Geophys. Res.*, *112*, A02203, doi:10.1029/2006JA012005.

Otto, A., M. S. Hsieh, and F. H. IV (2014), *Magnetotails in the Solar System*, chap. Current sheets in planetary magnetospheres, John Wiley, Hoboken, N. J.

Paranicas, C. P., B. H. Mauk, and S. M. Krimigis (1991), Pressure anisotropy and radial stress balance in the Jovian neutral sheet, *J. Geophys. Res.*, *96*, 21,135–21,140, doi:10.1029/91JA01647.

Radioti, A., D. Grodent, J.-C. Gérard, S. E. Milan, B. Bonfond, J. Gustin, and W. Pryor (2011), Bifurcations of the main auroral ring at Saturn: Ionospheric signatures of consecutive reconnection events at the magnetopause, *J. Geophys. Res.*, *116*, A11209, doi:10.1029/2011JA016661.

Radioti, A., E. Roussos, D. Grodent, J.-C. GéRard, N. Krupp, D. G. Mitchell, J. Gustin, B. Bonfond, and W. Pryor (2013), Signatures of magneto-spheric injections in Saturn's aurora, *J. Geophys. Res. Space Physics*, *118*, 1922–1933, doi:10.1002/jgra.50161.

Ray, L. C., R. E. Ergun, P. A. Delamere, and F. Bagenal (2010), Magnetosphere-ionosphere coupling at Jupiter: Effect of field-aligned potentials on angular momentum transport, *J. Geophys. Res.*, *115*, A09211, doi:10.1029/2010JA015423.

Russell, C. T., D. E. Huddleston, K. K. Khurana, and M. G. Kivelson (1999), Structure of the Jovian magnetodisk current sheet: Initial Galileo observations, *Planet. Space Sci.*, *47*, 1101–1109.

Rymer, A. M., D. G. Mitchell, T. W. Hill, E. A. Kronberg, N. Krupp, and C. M. Jackman (2013), Saturn's magnetospheric refresh rate, *Geophys. Res. Lett.*, *40*, 2479–2483, doi:10.1002/grl.50530.

Schindler, K., and J. Birn (2004), MHD stability of magnetotail equilibria including a background pressure, *J. Geophys. Res.*, *109*, A10208, doi:10.1029/2004JA010537.

Sergeev, V. A., V. Angelopoulos, and R. Nakamura (2012), Recent advances in understanding substorm dynamics, *Geophys. Res. Let*, *39*, L05101, doi:10.1029/2012GL050859.

Sergis, N., S. M. Krimigis, D. G. Mitchell, D. C. Hamilton, N. Krupp, B. M. Mauk, E. C. Roelof, and M. Dougherty (2007), Ring current at Saturn: Energetic particle pressure in Saturn's equatorial magnetosphere measured with Cassini/MIMI, *Geophys. Res. Lett.*, *34*, L09102, doi:10.1029/2006GL029223.

Sergis, N., S. M. Krimigis, D. G. Mitchell, D. C. Hamilton, N. Krupp, B. H. Mauk, E. C. Roelof, and M. K. Dougherty (2009), Energetic particle pressure in Saturn's magnetosphere measured with the Magnetospheric Imaging Instrument on Cassini, *J. Geophys. Res.*, *114*, A02214, doi:10.1029/2008JA013774.

Siscoe, G. L., and D. Summers (1981), Centrifugally driven diffusion of Iogenic plasma, *J. Geophys. Res.*, *86*, 8471–8479, doi:10.1029/JA086iA10p08471.

Southwood, D. J., and M. G. Kivelson (1987), Magnetospheric interchange instability, *J. Geophys. Res.*, *92*, 109–116, doi:10.1029/JA092iA01p00109.

Southwood, D. J., and M. G. Kivelson (2001), A new perspective concerning the influence of the solar wind on the Jovian magnetosphere, *J. Geophys. Res.*, *106*, 6123–6130, doi:10.1029/2000JA000236.

Southwood, D. J., and M. G. Kivelson (2007), Saturnian magnetospheric dynamics: Elucidation of a camshaft model, *J. Geophys. Res.*, *112*, A12222, doi:10.1029/2007JA012254.

Stallard, T. S., S. Miller, S. W. H. Cowley, and E. J. Bunce (2003), Jupiter's polar ionospheric flows: Measured intensity and velocity variations poleward of the main auroral oval, *Geophys. Res. Lett.*, *30*(5), 1221, doi:10.1029/2002GL016031.

Thomsen, M. F., D. B. Reisenfeld, D. M. Delapp, R. L. Tokar, D. T. Young, F. J. Crary, E. C. Sittler, M. A. McGraw, and J. D. Williams (2010), Survey of ion plasma parameters in Saturn's magnetosphere, *J. Geophys. Res.*, *115*, A10220, doi:10.1029/2010JA015267.

Thomsen, M. F., C. M. Jackman, R. L. Tokar, and R. J. Wilson (2014), Plasma flows in Saturn's nightside magnetosphere, *J. Geophys. Res. Space Physics*, *119*, 4521–4535, doi:10.1002/2014JA019912.

Vasyliunas, V. M. (1983), *Physics of the Jovian Magnetosphere*, chap. Plasma distribution and flow, pp. 395–453, Cambridge Planetary Science Series, Cambridge, New York.

Vogt, M. F., M. G. Kivelson, K. K. Khurana, S. P. Joy, and R. J. Walker (2010), Reconnection and flows in the Jovian magnetotail as inferred from magnetometer observations, *J. Geophys. Res.*, *115*, A06219, doi:10.1029/2009JA015098.

Vogt, M. F., M. G. Kivelson, K. K. Khurana, R. J. Walker, B. Bonfond, D. Grodent, and A. Radioti (2011), Improved mapping of Jupiter's auroral features to magnetospheric sources, *J. Geophys. Res.*, *116*, A03220, doi:10.1029/2010JA016148.

Vogt, M. F., M. G. Kivelson, K. K. Khurana, R. J. Walker, M. Ashour-Abdalla, and E. J. Bunce (2014), Simulating the effect of centrifugal forces in Jupiter's magnetosphere, *J. Geophys. Res. Space Physics*, *119*, 1925–1950, doi:10.1002/2013JA019381.

Went, D. R., M. G. Kivelson, N. Achilleos, C. S. Arridge, and M. K. Dougherty (2011), Outer magnetospheric structure: Jupiter and Saturn compared, *J. Geophys. Res.*, *116*, A04224, doi:10.1029/2010JA016045.

Wilson, R. J., P. A. Delamere, F. Bagenal, and A. Masters (2012), Kelvin-Helmholtz instability at Saturn's magnetopause: Cassini ion data analysis, *J. Geophys. Res.*, *117*, A03212, doi:10.1029/2011JA016723.

Wilson, R. J., F. Bagenal, P. A. Delamere, M. Desroche, B. L. Fleshman, and V. Dols (2013), Evidence from radial velocity measurements of a global electric field in Saturn's inner magnetosphere, *J. Geophys. Res. Space Physics*, *118*, 2122–2132, doi:10.1002/jgra.50251.

Wing, S., and J. R. Johnson (2010), Introduction to special section on Entropy Properties and Constraints Related to Space Plasma Transport, *J. Geophys. Res.*, *115*, A00D00, doi:10.1029/2009JA014911.

Woch, J., N. Krupp, and A. Lagg (2002), Particle bursts in the Jovian magnetosphere: Evidence for a near-Jupiter neutral line, *Geophys. Res. Lett.*, *29*(7), 1138, doi:10.1029/2001GL014080.

Wolf, R. A., C. X. Chen, and F. R. Toffoletto (2012), Thin filament simulations for Earth's plasma sheet: Interchange oscillations, *J. Geophys. Res.*, *117*, A02215, doi:10.1029/2011JA016971.

Young, D. T., et al. (2004), Solar wind interactions with Comet 19P/Borrelly, *Icarus*, *167*, 80–88, doi:10.1016/S0019-1035(03)00281-1.